

Reduction of turbulent mixing at the ablation front of fusion targets

H. Takabe and A. Yamamoto

Institute of Laser Engineering, Osaka University, Suita, Osaka 565, Japan

(Received 6 August 1990; revised manuscript received 2 January 1991)

The turbulent mixing generated at the surface of an inertial-confinement fusion target affected by the Rayleigh-Taylor instability is studied with the use of a simple, nonlinear diffusion model. In order to study the turbulent mixing at the ablation front, a reduced growth rate of the Rayleigh-Taylor instability is used in the model. It is found that, compared with the classical layered fluids, turbulent mixing at the ablation front is significantly suppressed because of the ablative stabilization effect. With the use of a constant-acceleration model, we conclude that targets imploded with an in-flight aspect ratio less than about 50 to 70 survive without suffering shell breakup as a result of the turbulent mixing.

PACS number(s): 52.50.Jm, 47.20. - k, 47.25.Jn

I. INTRODUCTION

Hydrodynamic stability is a key issue for achieving inertial-confinement fusion within a realistic range of driver energy. The Rayleigh-Taylor [1] and Richtmyer-Meshkov [2] instabilities can potentially degrade the target performance compared to that predicted by a one-dimensional simulation code. These instabilities can be triggered by nonuniformity in the irradiated intensity or by nonsphericity of the targets.

A variety of implosion experiments have been carried out with gas-filled targets [3,4], cryogenic targets [5], or deuterized polyethylene shell targets [6]. Results of these experiments have been compared in detail with predictions from one-dimensional fluid codes. The neutron yield, for example, differs by about a factor 2 to 10^3 for the case of gas targets [4], the difference arising mainly from the nonuniformity of the implosion dynamics.

Two-dimensional simulations have been carried out to explain the above discrepancy [5,7]. For example, a level of nonuniformity that produces a reduction of a factor 2 in neutron yield has been studied [7]. In that simulation, a nonuniformity of the $l=6$ mode is assumed in laser absorption. It is reported that a σ_{rms} of 35% in absorption nonuniformity is required. This level is too high. It is difficult to reduce the neutron yield by larger factors of 10^2 to 10^3 compared to a one-dimensional simulation if only the nonuniformity of relatively longer wavelength modes ($l \lesssim 24$) is included. It may be necessary to take into account the role of the instability for relatively shorter wavelength (e.g., $l \approx 100-500$). The instability growth of these short wavelengths is difficult to simulate with conventional two-dimensional implosion codes. Such perturbations grow very rapidly, becoming nonlinear in a short time, and mode coupling takes place. Through the mode coupling, the source of the instability for longer wavelengths is generated and the instability continues to grow. Such an inverse-cascading process in the spectra of turbulence may cause microscopic mixing of the contact surface, even without any imposed nonuniformity of the initial state.

In the present paper, we derive a simple, nonlinear diffusion model to describe time development of the mix-

ing layer by use of the quasilinear theory. We first apply this model to explain the mixing of classical layered fluids. Then, we use the model to evaluate the turbulent mixing near the ablation front accelerated by laser irradiation. Our main purpose is to estimate the degree of reduction in the growth of the mixing layer at the ablation front where the ablative stabilization affects the growth of the Rayleigh-Taylor instability.

In Sec. II, the scaling law of the turbulent mixing layer obtained experimentally by Read [8] is briefly described and compared with an earlier theoretical study by Belen'kii and Fradkin [9]. The inverse-cascading phenomena observed in the experiment are explained theoretically by considering the bubble coalescence phenomena. In Sec. III, we formulate a nonlinear diffusion equation that describes the turbulent diffusion phenomena according to the framework of the quasilinear theory. In a limiting case, we obtain the characteristic size and amplitude of eddies that predominantly controls the turbulent diffusion. The diffusion equation is solved for the classical layered fluid and it is shown that a scaling law similar to that by Read is obtained. Section IV is devoted to an estimation of the turbulent mixing at the ablation front accelerated by laser irradiation. The diffusion-type equation formulated in Sec. III is applied and a self-consistent growth rate, which includes the ablative stabilization effect, is used to see how the development of the turbulence is reduced. The main purpose of this paper is to estimate how high an in-flight aspect ratio is allowed when we require no shell breakup as a result of the turbulent mixing. This point is discussed by assuming a constant-acceleration model. Finally, Sec. V is devoted to a brief summary and conclusion.

II. TURBULENT MIXING PHENOMENA

The experimental result by Read [8] indicates that, even without any imposed initial perturbation, the contact surface of layered fluids that are Rayleigh-Taylor unstable tends to mix with a mixing distance $h(t)$ of the form

$$h(t) = 0.07 \alpha_A g t^2, \quad (1)$$

where α_A is the Atwood number, g is the effective acceleration, and t is the time. The experiment tested a variety of fluids with different densities, leading to Eq. (1), which is almost universally satisfied within a negligible deviation in a factor.

Such turbulent mixing has already been predicted by Belen'kii and Fradkin [9]. They have modeled the turbulent intermixing by the use of analogy with ordinary molecular mixing theory. They derived a diffusion-type equation for the density profile $\rho(x, t)$:

$$\frac{\partial}{\partial t} \rho = \frac{\partial}{\partial x} \left[D_t \frac{\partial}{\partial x} \rho \right], \quad (2)$$

where D_t is the turbulent diffusion coefficient and given to be

$$D_t = l_t^2 \epsilon \gamma, \quad (3)$$

with

$$\gamma = \left[-\frac{1}{\rho^2} \frac{\partial \rho}{\partial x} \frac{\partial P}{\partial x} \right]^{1/2}.$$

In Eq. (3), P is the pressure and $\epsilon=1$ for $(\partial \rho / \partial x)(\partial P / \partial x)$ negative and $\epsilon=0$ for $(\partial \rho / \partial x)(\partial P / \partial x)$ positive. They introduced a path length l_t and assumed the relation

$$l_t = C_1 h, \quad (4)$$

where h is the width of the intermixing region and C_1 is a constant. By solving Eq. (2), they obtained a relation

$$h(t) \propto g t^2. \quad (5)$$

This relation predicts the $g t^2$ dependence in Eq. (1). However, the α_A dependence in Eq. (1) cannot be predicted exactly because they used a local approximation in evaluating the growth rate γ in Eq. (3).

A numerical simulation has been carried out by Young [10] to explain the relation of Eq. (1). In his two-dimensional simulation, relatively shorter wavelength perturbations are imposed initially. It is seen that in the course of time, bubbles coalesce and the mixing layer is almost the size of the dominant bubbles. Such a phenomenon is also seen in Read's experiments both in two and three dimensions and the simulation resulted in a good agreement with Eq. (1). The reason for bubble coalescence, which is an alternative expression for the inverse-cascading described previously, can be understood as follows.

It is well known that the bubble-and-spike structure appears in the nonlinear stage of the Rayleigh-Taylor instability as shown schematically in Fig. 1. The penetration of the bubbles into the heavier fluid causes shell breakup and burnthrough of foils in the laser-driven ablative acceleration. The dynamics of bubbles was studied by Davies and Taylor [11]. Following their method, we study the rising velocity of a bubble which characterizes the nonlinear dynamics of the Rayleigh-Taylor instability.

Let us pick up one bubble from Fig. 1, which is shown

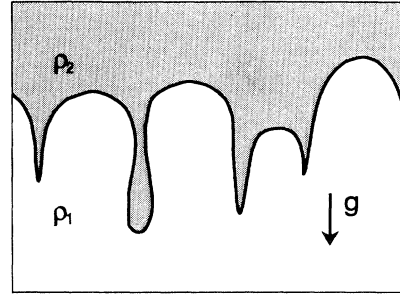


FIG. 1. Schematic figure of the bubble-and-spike structure seen in the nonlinear stage of the Rayleigh-Taylor instability.

in Fig. 2 as an idealized bubble, and assume that the bubble rises at a constant velocity U . Experiments [12] and model analysis [13] also show that a bubble rises with a constant velocity. Assuming a stationary state in the frame moving with the bubble and the incompressibility condition in the gravitational field g , we can use the Bernoulli theorem [14] for two-dimensional flow:

$$P + \frac{1}{2} \rho q^2 + \rho g x = P_0, \quad (6)$$

where q is the flow velocity, P the pressure, ρ the fluid density, and x is the vertical axis with $x=0$ at the vertex of the bubble. In Eq. (6), P_0 is a constant equal to the pressure at the vertex of the bubble, and Eq. (6) is satisfied by the fluids on the bubble surface.

In the case where the bubble is axially symmetric along the x axis [three-dimensional (3D) bubble], the flow of the heavier fluid near the bubble surface can be given by the flow near the surface of a sphere in a stream [11]. Then, the flow velocity on the surface is given to be [15]

$$q = \frac{3}{2} U \sin \theta, \quad (7)$$

where θ is the angle from the x axis (see Fig. 2). The flow velocity is equal to zero ($q=0$) at the stagnation point $\theta=0$.

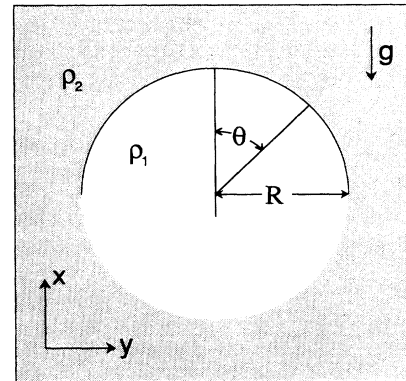


FIG. 2. Schematic figure of a bubble rising in the heavier fluid with the radius of R . This can model the penetration of bubbles into the heavier fluids in the nonlinear stage of the Rayleigh-Taylor instability shown in Fig. 1.

On the other hand, for the fluids in the bubble Eq. (6) reduces to

$$P - P_0 = \rho_1 g x, \quad (8)$$

where ρ_1 is the density of the lighter fluid. In deriving Eq. (8), we have assumed $q=0$ in the moving frame. Equation (6) for the heavier fluid leads to

$$P_0 - P = \frac{1}{2}\rho_2 q^2 + \rho_2 g x, \quad (9)$$

where ρ_2 is the density of the heavier fluid. Since the pressures should balance on the surface, Eqs. (8) and (9) yield

$$q = \left[-\frac{\rho_2 - \rho_1}{\rho_2} g x \right]^{1/2}. \quad (10)$$

By the use of the relation that the flow velocity of Eq. (7) should be equal to that of Eq. (10) in the vicinity of the vertex, we can obtain the rising velocity U in the form

$$U = \frac{2}{3} \left[\left[\frac{\rho_2 - \rho_1}{\rho_2} g R \right]^{1/2} \right] \propto R^{1/2}, \quad (11)$$

where R is the radius of the bubble. To obtain Eq. (11), we have used the approximation near the vertex of the spherical bubble, $x = (1 - \cos\theta)R \simeq (-\theta^2/2)R$ and $\sin\theta \simeq \theta$. Equation (11) indicates that larger bubbles rise faster. It is noted that in the limit of $\rho_2 \gg \rho_1$, Eq. (11) reduces to the Davies-Taylor formula [11].

It is useful to derive Eq. (11) by an intuitive way for understanding the physics behind it. In the frame moving with the bubble, the three forces acting on the bubble should balance; the first one is the buoyancy, the second one is the gravitational force, and the third one is the drag force due to the heavier fluid flow. The combined force of the first and the second forces (call it the effective buoyancy, B) is

$$B = (\rho_2 - \rho_1)gV, \quad (12)$$

where V is the volume of the bubble. On the other hand, the drag force is due to the obstruction against the heavier fluid flow and is equal to the change of the momentum of the heavier fluid per unit time by the bubble obstruction; therefore the drag force F_d

$$F_d \approx \rho_2 U^2 S, \quad (13)$$

where S is the area of the bubble seen by the heavier fluid flow. It is reasonable to assume the relation $V \propto R^3$ and $S \propto R^2$. By the use of the relation that Eq. (12) should balance Eq. (13), we can obtain Eq. (11) again except for the numerical coefficient.

The turbulence in the mixing region driven by the Rayleigh-Taylor instability has a different feature compared to the uniform turbulence driven, for example, in the Couette flow. The buoyancy of the bubble plays an essential role in the time evolution of the turbulence spectra. The Rayleigh-Taylor instability is the process by which the excess potential energy is released as energies

of fluid motion. Since the rate of the release is proportional to the rise velocity of bubbles, the bubbles tend to coalesce with each other and increase their rise velocities. In other words, the bubble coalescence due to bubble-bubble collision corresponds to the inverse cascading due to mode-mode coupling because the size of bubble R is roughly proportional to the wavelength of the Rayleigh-Taylor mode λ . In this meaning, the inverse cascading might be observed in the turbulent mixing layer.

It is also useful to repeat the same thing done above for the case of the two-dimensions. It is observed in Read's experiment that the mixing layer grows slightly slower in the 2D geometry than in the 3D geometry. However, he found no qualitative difference and instead of Eq. (1) he obtained

$$h(t) = 0.06 \alpha_A g t^2.$$

If the bubble in Fig. 2 is two-dimensional in the planar geometry (uniform in the z direction), then the flow velocity on the surface is given in the form [15]

$$q = 2U \sin\theta. \quad (14)$$

Equation (10) is also applicable in this case and we obtain

$$U = \frac{1}{2} \left[\frac{\rho_2 - \rho_1}{\rho_2} g R \right]^{1/2}. \quad (15)$$

Within the present model, the difference between 3D and 2D is just the difference in the numerical coefficients of Eqs. (11) and (15), and bubbles rise slightly slower in 2D than in 3D. This fact might explain the slower growth of the mixing layer in 2D observed in the Read's experiment.

It should be noted that the bubble coalescence (inverse cascade) may take place in both 2D and 3D and there may be no qualitative difference between 2D and 3D as far as the Rayleigh-Taylor instability is concerned. In this regard, the phenomenon is very different from the uniform turbulence where the inverse cascade occurs only in 2D and the normal cascade occurs in 3D because of the stretching of the vortex lines until the vortex energy is dissipated by viscosity or some other dissipation mechanism. When we see bubbles generated by the Rayleigh-Taylor instability, the Kelvin-Helmholtz instability and the stretching of the vortex generate smaller size vortices and the cascade process may be dominant there. However, the total energy of the vortices in the mixing layer continues to increase because of the excess gravitational energy. Therefore it is not unreasonable to assume that most of the vortex energy is associated with bubbles getting bigger due to the bubble coalescence as described above.

It is useful to study at what point the linear Rayleigh-Taylor instability enters into the nonlinear phase described above. When a 2D sinusoidal perturbation of the contact surface $x(y, t)$ is growing as $x(y, t) = \xi \cos(ky)$, where $\xi = \xi_0 e^{\gamma t}$ and ξ_0 is an initial amplitude, the radius of curvature at the vertex of the perturbation is calculated to be $R_s = (\xi k^2)^{-1}$. The vertex rises in the linear phase at the velocity $u = \gamma \xi$. However, the velocity u cannot exceed the rising velocity U of Eq. (15) with R re-

placed by R_s , because the nonlinear drag force of Eq. (13) which is proportional to u^2 appears to be dominant and prohibits further exponential growth. The boundary between the linear and nonlinear regimes can be roughly estimated by the relation

$$u = U .$$

That is,

$$k\xi = 0.63 \left(\frac{\rho_2 + \rho_1}{\rho_2} \right)^{1/3} . \quad (16)$$

This indicates that the Rayleigh-Taylor instability enters into the nonlinear phase when the amplitude grows up to $k\xi \approx 1$. For the case $\rho_2 \gg \rho_1$, $k\xi = 0.63$ and $\xi = 0.1\lambda$. At this amplitude, the radius of curvature is $R_s \approx \lambda/4$. In the case of 3D with $k_y = k_z = \sqrt{2}k$, Eq. (11) is applicable. Since $R_s = (\xi k_y^2)^{-1}$ in this case, we obtain

$$k\xi = 0.96 \left(\frac{\rho_2 + \rho_1}{\rho_2} \right)^{1/3} . \quad (16')$$

It is clear that the Rayleigh-Taylor instability in 3D enters into the nonlinear phase with larger amplitude than that in 2D for the same value of k . This tendency coincides with the numerical results shown in Ref. [16], although the geometry of Ref. [16] is different from the plane geometry.

Recently, Emery [17] has carried out a simulation and shown the inverse-cascading phenomena due to the Rayleigh-Taylor instability at the ablation front accelerated by laser irradiation. He reported a reduced growth of the mixed layer compared to that of the non-ablative surface. Haan [18] has dealt with multimode Rayleigh-Taylor growth and proposed a model for evaluating the time development of the mixing layer. In his model, all modes are assumed to grow independently and mode coupling is not explicitly taken into account. Each mode grows exponentially in the linear phase and grows very slowly in a nonlinear saturation phase. Because of the slow growth in the nonlinear phase, longer wavelength modes with higher saturation amplitude become predominant in time. As a result, the wave number corresponding to the peak in the multimode spectra tends to decrease and an inverse cascading is observed as a result. The result by Read is also explained by Haan's model.

In order to model the turbulent mixing qualitatively, a multiflow model [10] or a turbulent viscosity model [19] has also been used. However, applying these models to turbulent mixing at the ablation front being accelerated by laser light is not straightforward. Therefore we introduce a simple model that can explain Eq. (1) and apply it to the turbulent mixing at the ablation front.

III. NONLINEAR DIFFUSION MODEL

Consider the situation where two fluids with different densities are present in a gravitational field. The contact surface tends to be unstable, as seen in Fig. 3. The figure also shows the density structure averaged in the y direc-

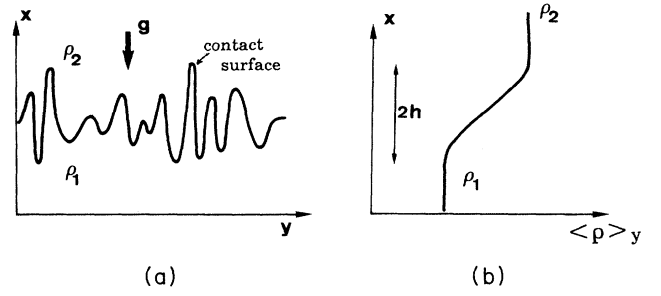


FIG. 3. (a) Schematic figure of the deformation of the contact surface that is unstable to the Rayleigh-Taylor instability. The quantity g is the effective acceleration. (b) The density profile averaged over the y direction, where $2h$ is the thickness of the mixing layer.

tion. The equation of continuity averaged over the y direction reduces to

$$\frac{\partial}{\partial t} \rho_0(x, t) + \frac{\partial}{\partial x} \langle \rho_1 u_x \rangle_y = 0 , \quad (17)$$

where $\langle \rangle_y$ means the average in the y direction and $\rho = \rho_0 + \rho_1$ and $\rho_0 = \langle \rho \rangle_y$. The density perturbation ρ_1 is given by the linearized equation of continuity:

$$\rho_1 = -\xi \frac{\partial}{\partial x} \rho_0 , \quad (18)$$

where we have assumed the fluid motion is incompressible. In Eqs. (17) and (18), the velocity perturbation of flow in the x direction, u_x , is related to the displacement in the x direction, ξ by $u_x = d\xi/dt (\equiv \dot{\xi})$.

Inserting Eq. (18) in Eq. (17), we obtain an equation for ρ_0 that is of the diffusion type:

$$\frac{\partial}{\partial t} \rho_0 = \frac{\partial}{\partial x} D \frac{\partial}{\partial x} \rho_0 , \quad (19)$$

$$D = \langle \xi \dot{\xi} \rangle_y .$$

The nonlinear diffusion coefficient can be rewritten with spectral density $|\xi_k|^2$, where $\xi = \int_{-\infty}^{\infty} \xi_k e^{iky} dk$:

$$D = \frac{2\pi}{L} \int_{-\infty}^{\infty} dk \gamma_k |\xi_k|^2 . \quad (20)$$

Here, L is the size for sampling in the y direction and k is the wave number in the y direction. Note that the diffusion coefficient is proportional to the linear growth rate γ_k of the perturbations.

In solving Eq. (19), we assume that the turbulence spectra has a strong peak near the wave number k_0 and, therefore,

$$D \approx \gamma_k |\xi_k|^2 |_{k=k_0} . \quad (21)$$

The analysis in Ref. [20] supports this assumption. Inserting the classical growth rate $\gamma_k = (\alpha_A kg)^{1/2}$ in Eq. (19) and assuming that $\xi_k \propto h$, where h is the mixing distance and $k \propto h^{-1}$, we obtain an important relation from simple dimensional analysis:

$$h \simeq (Dt)^{1/2} \simeq \alpha_A g t^2 . \quad (22)$$

Equation (22) agrees with Eq. (1) except for the dimensionless factor 0.07. Note that the derivation of Eq. (22) suggests that the mixing distance is proportional to the square of the growth rate of the Rayleigh-Taylor (RT) instability

$$h \propto \gamma_k^2 . \quad (23)$$

Equation (19) together with the diffusion coefficient of Eq. (21) agrees with Eq. (2), if we assume the relation $|\xi_{k0}| = l_t$ and $\gamma_{k0} = \gamma$ in Eq. (3). This agreement results although we started from a different standing point. The dimensional analysis provides the same results as Eqs. (5) and (22) except for the α_A dependence in Eq. (22). This is because the local approximation is used for the growth rate in Eq. (3). Note that Equation (20) is more general and useful if we simultaneously solve the multimode spectra such as discussed in Ref. [18].

The factor 0.07 of Eq. (1) can be derived by solving Eq. (19) numerically. We introduce numerical constants a and b defined by

$$\begin{aligned} \xi_k &= ah , \\ k &= b/h . \end{aligned} \quad (24)$$

Then, for the classical growth rate $\gamma = (\alpha_A kg)^{1/2}$, Eq. (19) reduces to

$$\frac{\partial}{\partial \tau} \rho_0 = \frac{\partial}{\partial x} [h(t)]^{3/2} \frac{\partial}{\partial x} \rho_0 , \quad (25)$$

where

$$\tau = (\alpha_A gb)^{1/2} a^2 t .$$

In solving Eq. (25), we start with the initial profile

$$\rho_0 = \begin{cases} \rho_1, & x < 0 \\ \rho_2, & x > 0 \end{cases} \quad (26)$$

and $h(t)$ is calculated at each time by best fitting the density profile to the profile used in Ref. [20]

$$\rho_0 = \begin{cases} \rho_1 & (x < -h) \\ \frac{1}{2}(\rho_1 + \rho_2) + \frac{1}{2}(\rho_2 - \rho_1)x/h & (-h \leq x \leq h) \\ \rho_2 & (h < x) . \end{cases} \quad (27)$$

The density profile is correctly determined if the nonlinear diffusion coefficient, which is the product of the growth rate and local density of the turbulence, is explicitly given. In Ref. [9], the local approximation to the growth rate is used to give an explicit form of the diffusion coefficient. However, nonlocal effects are an essential property in the Rayleigh-Taylor mode structure. Although nonlocal effects are important to determine the density profile of the mixed layer, it is out of the scope of the present paper. Therefore we simply assume the density profile of Eq. (27).

Solving Eq. (25) numerically, we obtain the relation

$$h(t) = 1.9\tau^2 . \quad (28)$$

In addition, following the method described by Mikaelian [20], we use the energy-conservation relation to balance the released potential energy with the kinetic energy of the eddies:

$$\begin{aligned} \left[\int_{-h}^0 \rho_1 g x dx + \int_0^h \rho_2 g x dx \right] - \int_{-h}^h \rho_0(x) g x dx \\ = \int_{-h}^h \frac{1}{2} \rho_0 \langle u^2 \rangle dx . \end{aligned}$$

This reduces to the relation

$$\frac{1}{6} g (\rho_2 - \rho_1) h^2 = \frac{1}{2} (\rho_2 + \rho_1) \alpha_A b g a^2 h^2 . \quad (29)$$

In order to obtain the potential energy, the left-hand side of Eq. (29), we assumed the density structure of Eq. (27).

By requiring that Eq. (28) is equal to Eq. (1) and using Eq. (29), we can obtain the unknown parameters a and b as

$$\begin{aligned} a &= 0.33 , \\ b &= 3.0 . \end{aligned} \quad (30)$$

This means the wavelength and amplitude of the eddies are $\lambda \approx 2h$ and $k\xi \approx 1$, respectively. It is useful to note that the dominant mode is always around the marginal point between linear and nonlinear phases where Eq. (16') is approximately satisfied.

IV. REDUCED TURBULENT MIXING IN ABLATIVE TARGET ACCELERATION

In inertial-confinement fusion, acceleration of a spherical shell target should be stable enough to realize central convergence. Suppose that a target of initial radius R_0 with the thickness ΔR_0 is accelerated halfway to the center within the acceleration time t_A . If the acceleration is almost constant, we can assume a simple relation

$$gt_A^2 = R_0 , \quad (31)$$

where g is the acceleration. In general, the target is initially compressed by shock waves and the thickness of the target is usually smaller than ΔR_0 . We assume that the in-flight thickness is given as ΔR_{inf} and is almost constant in time. In order to avoid shell breakup as a result of turbulent mixing during the acceleration time, the mixing distance at $t = t_A$, $h(t_A)$, is required to be less than the in-flight shell thickness, namely,

$$h(t_A) < \Delta R_{\text{inf}} . \quad (32)$$

In the design of inertial-confinement fusion (ICF) targets, the in-flight aspect ratio A_{inf} , which is here defined by $A_{\text{inf}} = R_0 / \Delta R_{\text{inf}}$, is used as a measure for stability. Equation (22) is equivalently replaced by the following requirement for the in-flight aspect ratio:

$$A_{\text{inf}} < \frac{R_0}{h(t_A)} . \quad (33)$$

If the Rayleigh-Taylor instability in the acceleration phase were classical and the mixing distance were given by Eq. (1), then Eq. (33) reduces to the relation

$$A_{\text{inf}} < 14. \quad (34)$$

In obtaining Eq. (34), we used Eq. (31) and assumed $\alpha_A = 1$. The in-flight aspect ratio that satisfies Eq. (34) is much lower than those expected in usual target design for high gains [21,22]. In general, the hydrodynamic efficiency decreases with the decrease of the in-flight aspect ratio. In addition, the required laser intensity increases and an unwelcome nonlinear effect appears to be important in the laser-plasma interaction process [21]. In fact, however, the Rayleigh-Taylor instability at the ablation front is not that of usual layer fluids, but a significant reduction in the growth rate of the instability has been reported by many authors by the way of eigenvalue analysis in self-consistent structure [23,24], two-dimensional simulations with improved numerical schemes [25–29], or model analysis [30–32]. It is, therefore, necessary to see how this stabilization effect reduces the growth of the turbulent mixing layer.

If the growth rate is reduced by a factor ϵ on average compared with the classical $(kg)^{1/2}$, Eq. (34) can be modified as

$$A_{\text{inf}} < \frac{14}{\epsilon^2}. \quad (35)$$

In obtaining Eq. (35), we used Eq. (23). Therefore, for the value of $\epsilon = 0.3$, the criterion is improved to $A_{\text{inf}} < 150$ and it becomes relatively easy to design high-gain targets. For more consistent evaluation we use the self-consistent growth rate [23]

$$\gamma = \alpha \sqrt{kg} - \beta k v_0, \quad (36)$$

where $\alpha = 0.9$ and $\beta = 3$ to 4. In Eq. (36), v_0 is the mass ablation velocity and given to be $v_0 = \dot{m} / \rho_a$, where \dot{m} is the mass ablation rate and ρ_a is the peak density at the ablation front. Note that Eq. (36) has become widely accepted as a result of accord among two-dimensional simulations [33–35]. In using Eq. (36), we need to evaluate the ablation velocity v_0 . For this purpose, we assume the following relation:

$$v_0 t_A = f \Delta R_{\text{inf}}, \quad (37)$$

where f is a fraction of the ablated mass to the initial mass of the target and is less than unity. Using Eqs. (31) and (37) and neglecting the effect of spherical geometry, Eq. (36) can be reduced to the form

$$\gamma = \left[\alpha \sqrt{k R_0} - \beta k R_0 \frac{f}{A_{\text{inf}}} \right] \frac{1}{t_A}. \quad (38)$$

This indicates that for a given f , the target design with reduced in-flight aspect ratio enhances the ablative stabilization effect.

Equation (38) is used in solving Eq. (19) together with the diffusion coefficient of Eq. (21). In solving Eq. (19), we use Eq. (24) for ξ_k and assume that the dominant wave number k is given as the minimum of b/h and k_m , where k_m is the wave number at which the growth rate in Eq. (38) has the maximum. This assumption is reasonable because the mode with $k = k_m$ is the predominant

growing mode initially. Note that the spherical wave number corresponding to k_m , $l_m = R_0 k_m$, is given to be $l_m = [\alpha A_{\text{inf}} / (2\beta f)]^2 = 0.05 A_{\text{inf}}^2$ for $\beta = 3.5$ and $f = \frac{2}{3}$. That is, $l_m = 2000, 500$, and 125 for $A_{\text{inf}} = 200, 100$, and 50 , respectively.

By employing a normalization

$$\frac{h}{R_0} = \tilde{h}, \quad \frac{x}{R_0} = \tilde{x}, \quad \frac{t}{t_A} = \tilde{t}, \quad (39)$$

Eq. (19) with Eqs. (21) and (24) can be reduced to the form:

$$\frac{\partial}{\partial \tilde{t}} \rho_0 = \frac{\partial}{\partial \tilde{x}} \tilde{D} \frac{\partial}{\partial \tilde{x}} \rho_0, \quad (40)$$

where

$$\tilde{D} = \alpha b^{1/2} a^2 \times \begin{cases} \tilde{h}^{2/3} - b^{1/2} \frac{1}{\alpha s} \tilde{h} & \text{for } \tilde{h} > \frac{b}{l_m} \\ \frac{b^{-1/2}}{4} s \tilde{h}^2 & \text{for } \tilde{h} < \frac{b}{l_m} \end{cases}, \quad (41)$$

and

$$s = \frac{A_{\text{inf}}}{\beta f}.$$

In solving Eq. (40), we assume a and b are given by Eq. (30), although it is not clear at the present time that Eq. (30) is applicable to the turbulence at the ablation front.

For a given value of s , Eq. (40) can be solved numerically. In Fig. 4, the time development of the distance of the mixing layer is shown for the cases of in-flight aspect ratio equal to 200, 100, and 70, where in evaluating s , we assumed $\beta = 3.5$ and $f = \frac{2}{3}$. In Fig. 4, the dash-dotted line is for the classical growth rate $(kg)^{1/2}$ instead of Eq. (36). By comparison, we see that the development of the mixing layer is drastically reduced for relatively lower in-flight aspect ratio.

In Fig. 5, the distance of the mixing layer at $t = t_A$ is

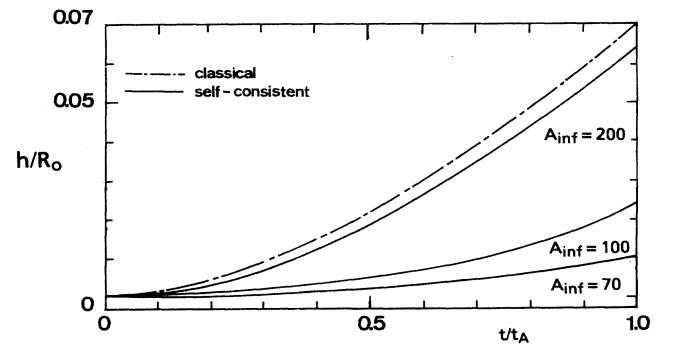


FIG. 4. Time development of the mixing layer h at the ablation front of accelerated targets with different in-flight aspect ratio. A_{inf} is the in-flight aspect ratio and the dash-dotted line represents the case in which the classical growth rate $\gamma = (kg)^{1/2}$ is used.

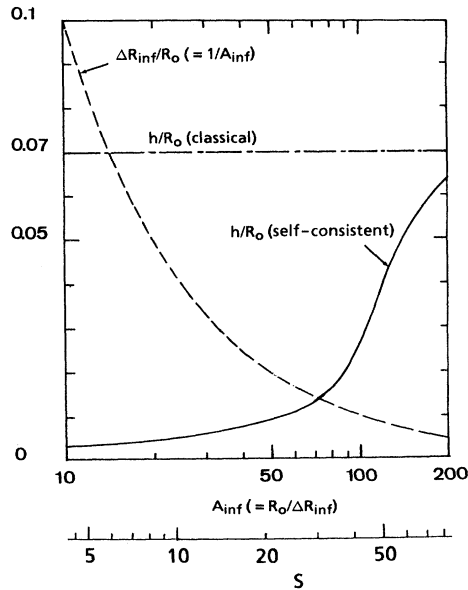


FIG. 5. The growth distance of the mixing layer as a function of the parameter s or the in-flight aspect ratio A_{inf} . The solid line is the case estimated with the self-consistent growth rate of the Rayleigh-Taylor instability, while the dash-dotted line is the case with the classical growth rate $\gamma = (kg)^{1/2}$. The dashed curve represents the thickness of the shell in flight. The figure indicates that an implosion with $A_{inf} < 50$ to 70 can survive without suffering shell breakup.

shown with the solid line as a function of the parameter s . For comparison, the mixing distance for the classical growth rate given in Eq. (1) is plotted by the dash-dotted line for the assumed value of $\alpha_A = 1$. It is clearly seen that a decrease of s , which corresponds to the increase of the ablative stabilization, leads to a drastic reduction in the growth of the turbulent mixing layer at the ablation front. For given values of β and f , the horizontal axis is replaced by the in-flight aspect ratio. The value of the in-flight aspect ratio for the case with $\beta = 3.5$ and $f = \frac{2}{3}$ is shown in the figure. The choice of $f = \frac{2}{3}$ is appropriate from a point of keeping the hydrodynamic efficiency high enough. A simple rocket model [36] yields that the hydrodynamic efficiency is only a function of f and it has a maximum at about $f = 0.8$. In the figure, the in-flight thickness of the target is also plotted with the dashed

line. It is found from this figure that the requirement for avoiding shell break up, which is defined by Eq. (32), restricts the target design to an in-flight aspect ratio less than about 70. $A_{inf} < 50$ may be required to take account of a safety factor.

V. SUMMARY AND CONCLUSION

We have introduced a simple, nonlinear diffusion equation describing the turbulent mixing phenomena. The equation, which is based on the quasilinear theory, explains the scaling law obtained experimentally by Read [8]. In the limit of narrow turbulence spectra, the diffusion equation has the same form as that obtained with the analogy to molecular diffusion equation. The nonlinear diffusion equation shows that the thickness of the turbulent mixing layer is proportional to the square of the growth rate of the Rayleigh-Taylor instability. Using this equation, we studied how ablative stabilization reduces the growth of turbulent mixing in the ablation front region.

Within a simple estimate for a constant-acceleration model, we have evaluated the condition under which shell breakup does not take place as a result of turbulent mixing. This condition requires an in-flight aspect ratio less than 14, if we use the classical growth rate $\gamma = (kg)^{1/2}$. It is found, however, that ablative stabilization relaxes this condition and targets imploded with an in-flight aspect ratio less than about 50 to 70 survive without suffering shell breakup as a result of turbulent mixing.

In the present paper, we did not take account of feedback to the growth rate from the density modification by diffusion. There should be some reduction in the growth of the instability due to the resultant diffused structure of the density. In addition, such diffusion possibly increases the effective ablation velocity because mass diffusion flux is additional to the one-dimensional mass ablation flux. This may enhance the ablative stabilization effect, consequently relaxing the restriction on the target design.

ACKNOWLEDGMENTS

The authors would like to express their thanks to Professor K. Mima, Professor K. Nishihara, and Professor S. Nakai for valuable discussions.

- [1] S. Chandrasekhar, *Hydrodynamic and Hydromagnetic Stability* (Oxford, London, 1961).
- [2] R. D. Richtmyer, *Commun. Pure. Appl. Math.* **13**, 297 (1960).
- [3] M. C. Richardson, P. W. McKenty, F. J. Marshall, C. P. Verdon, J. M. Soares, R. L. McCrory, O. Barnouin, R. S. Craxton, J. Delettrez, R. L. Hutchison, P. A. Jaanimagi, R. Keck, T. Kessler, H. Kim, S. A. Letzring, D. M. Roback, W. Seka, S. Skupsky, and B. Yaakobi, in *Laser Interaction and Related Plasma Phenomena*, edited by H.

Hora and G. H. Miley (Plenum, New York, 1986), Vol. 7, p. 179.

- [4] H. Takabe, M. Yamanaka, K. Mima, C. Yamanaka, H. Azechi, N. Miyanaga, M. Nakatsuka, T. Jitsuno, T. Norimatsu, M. Takagi, H. Nishimura, M. Nakai, T. Yabe, T. Sasaki, K. Yoshida, K. Nishihara, Y. Kato, Y. Izawa, T. Yamanaka, and S. Nakai, *Phys. Fluids* **31**, 2884 (1988).
- [5] F. J. Marshall, S. A. Letzring, C. P. Verdon, S. Skupsky, R. L. Keck, J. P. Knauer, R. L. Kremens, D. K. Bradley, T. Kessler, J. Delettrez, H. Kim, J. M. Soares, and R. L.

- McCrorry, *Phys. Rev. A* **40**, 2547 (1989).
- [6] S. Nakai, K. Mima, H. Azechi, N. Miyanaga, and A. Nishiguchi, in *Laser Interaction and Related Plasma Phenomena* (Plenum, New York, in press), Vol. 9.
- [7] H. Takabe, in *Short Wavelength Lasers*, edited by C. Yamanaka (Springer-Verlag, Berlin, 1988), p. 307; H. Takabe, K. Mima, and S. Nakai, *Laser Part. Beams* **7**, 175 (1989).
- [8] K. I. Read, *Physica D* **12**, 45 (1984).
- [9] S. Z. Belen'kii and E. S. Fradkin, *Proc. P. N. Lebedev Phys. [Acad. Sci. USSR]* **29**, 197 (1967).
- [10] D. L. Young, *Physica D* **12**, 32 (1984); **37**, 270 (1989).
- [11] R. M. Davies and G. I. Taylor, *Proc. R. Soc. London Ser. A* **200**, 375 (1950).
- [12] H. W. Emmons, C. T. Chang, and B. C. Watson, *J. Fluid Mech.* **7**, 177 (1960).
- [13] P. R. Garabedian, *Proc. R. Soc. London Ser. A* **241**, 423 (1957).
- [14] For example, L. D. Landau and E. M. Lifshitz, *Fluid Mechanics* (Pergamon, Oxford, 1959), Sec. 5.
- [15] See problems in Sec. 10 of Ref. [14].
- [16] H. Sakagami and K. Nishihara, *Phys. Rev. Lett.* **65**, 432 (1990); *Phys. Fluids B* **2**, 2715 (1990).
- [17] M. Emery, in *Laser Interaction and Related Plasma Phenomena*, edited by H. Hora and G. H. Miley (Plenum, New York, 1988), Vol. 8, p. 401.
- [18] S. Haan, *Phys. Rev. A* **39**, 5812 (1989).
- [19] V. A. Andronov, S. M. Bakharkh, E. E. Meshkov, V. V. Nikiforov, A. V. Pevnitskii, and A. I. Tolshmyakov, *Dokl. Akad. Nauk SSSR* **264**, 76 (1982) [*Sov. Phys.—Dokl.* **27**, 393 (1982)].
- [20] K. O. Mikaelian, *Physica D* **36**, 743 (1989); *J. Appl. Phys.* **65**, 964 (1989); *Phys. Fluids A* **2**, 592 (1990).
- [21] J. H. Gardner and S. E. Bodner, *Phys. Fluids* **29**, 2672 (1986).
- [22] S. M. Pollaine and J. D. Lindl, *Nucl. Fusion* **26**, 1719 (1986).
- [23] H. Takabe, L. Montierth, and R. L. Morse, *Phys. Fluids* **26**, 2299 (1983).
- [24] H. Takabe, K. Mima, L. Montierth, and R. L. Morse, *Phys. Fluids* **28**, 3676 (1985).
- [25] R. L. McCrorry, L. Montierth, R. L. Morse, and C. P. Verdon, *Phys. Rev. Lett.* **46**, 336 (1981).
- [26] C. P. Verdon, R. L. McCrorry, R. L. Morse, G. R. Baker, D. I. Meiron, and S. A. Orszag, *Phys. Fluids* **25**, 1653 (1982).
- [27] M. H. Emery, J. H. Gardner, and J. P. Boris, *Appl. Phys. Lett.* **41**, 808 (1982); **48**, 1406(E) (1986).
- [28] M. H. Emery, J. H. Gardner, and S. E. Bodner, *Phys. Rev. Lett.* **57**, 703 (1986).
- [29] M. H. Emery, J. P. Dahlburg, and J. H. Gardner, *Phys. Fluids* **31**, 1007 (1988).
- [30] S. E. Bodner, *Phys. Rev. Lett.* **33**, 761 (1974).
- [31] L. Baker, *Phys. Fluids* **21**, 295 (1978); **26**, 627 (1983).
- [32] H. J. Kull and S. I. Anisimov, *Phys. Fluids* **29**, 2067 (1986).
- [33] J. H. Gardner, S. E. Bodner, and J. P. Dahlburg, *Phys. Fluids B* **3**, 1070 (1991).
- [34] *LLE Rev. Lab. Laser Energ., Univ. Rochester* **37**, 2 (1988).
- [35] M. Tabak, D. H. Munro, and J. D. Lindl, *Phys. Fluids B* **2**, 1007 (1990).
- [36] R. Decoste, S. E. Bodner, R. H. Ripin, E. A. McLean, S. P. Obenschain, and C. M. Armstrong, *Phys. Rev. Lett.* **42**, 1673 (1979).